

ABSTRACT

Regularization stabilizes the geophysical imaging problem resulting from sparse and noisy measurements that render solutions unstable and non-unique. Regularization constraints in cascaded time-lapse (CTL) imaging of solute plumes are, however, independent of the transport physics and often produce smoothed-out tomograms with mass underestimation.

The proper orthogonal decomposition (POD)-constrained inversion framework, in contrast, enforces physics-based regularization based upon prior understanding of the expected evolution of state variables. We apply the algorithm to 2-D lab-scale saline transport experiments with electrical resistivity (ER) monitoring.

We compare POD difference tomograms with those obtained from CTL. Qualitative comparisons of the difference tomograms with images of their corresponding dye plumes suggest that POD recovered more compact plumes with fewer artifacts compared to those reconstructed with traditional CTL.

POD is computationally superior requiring less than 5 mins to complete each inversion compared to about 3 hours for CTL to do same.

TIME-LAPSE INVERSION FRAMEWORKS

CASCADED TIME-LAPSE (CTL) INVERSION

❖ The background tomogram (\mathbf{m}_0) is employed as starting model for the inversion of each subsequent time-lapse dataset.

❖ The CTL inversions are based on a combination of the traditional smallness and smoothness regularization on model parameters (\mathbf{m}) [e.g., *Pidlisecky et al., 2007*].

$$E(\mathbf{m}) = \|\mathbf{V}_{obs} - f_g(\mathbf{m})\|_2 + \beta \|\mathbf{W}(\mathbf{m} - \mathbf{m}_0)\|_2$$

where, \mathbf{V}_{obs} = observed data; f_g = resistivity forward operator; β =regularization parameter; and \mathbf{W} = regularization operator.

POD-BASED TIME-LAPSE (PODTL) INVERSION

❖ The POD-based inversion (*Oware et al., 2013*) proceeds in four major steps as illustrated in Figure 1.

❖ For PODTL (monitoring), coefficients (\mathbf{c}_0) of the background tomogram are employed as starting coefficients for the inversion of each subsequent time-lapse dataset.

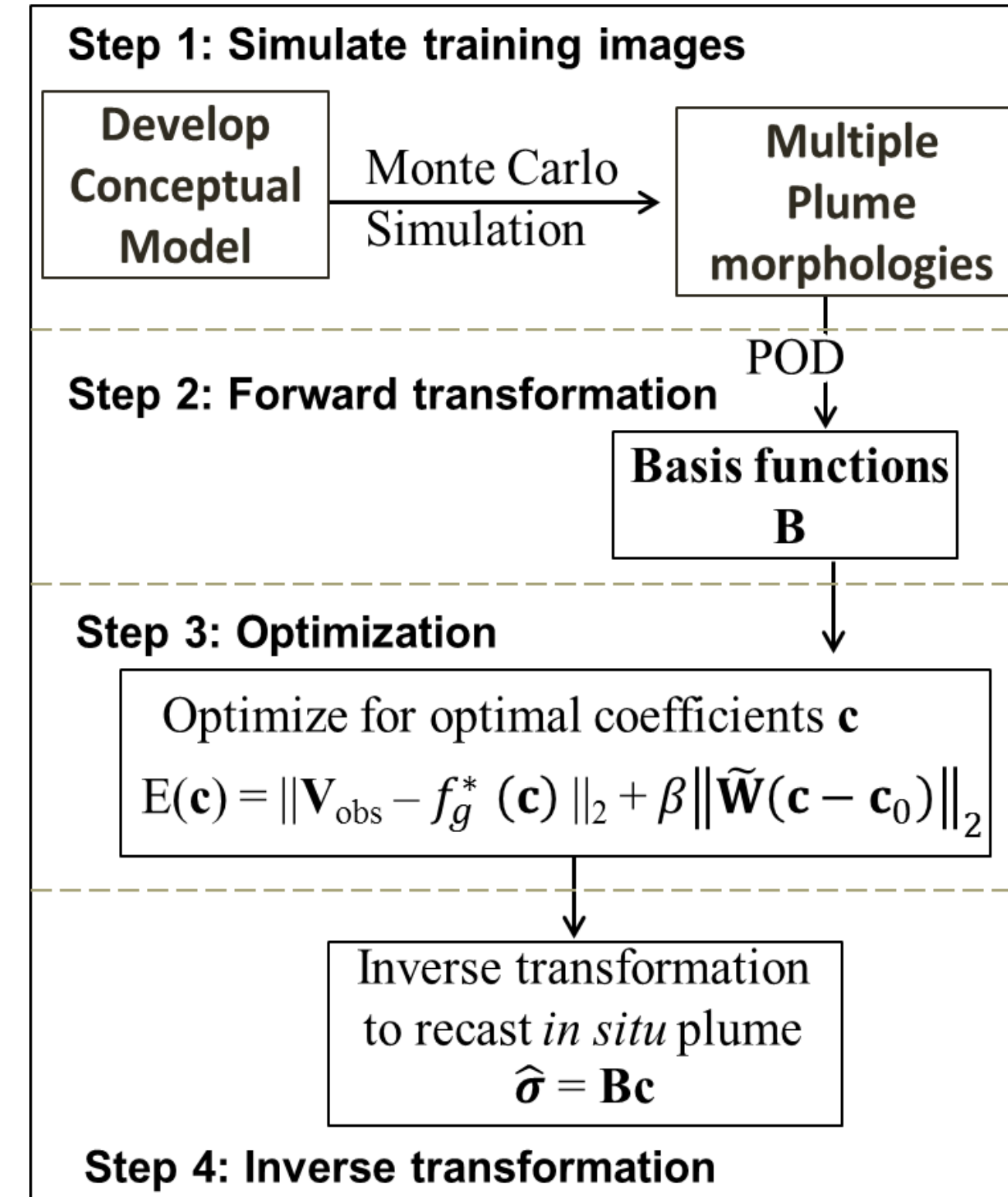


Figure 1: Flow chart of the POD-based inversion algorithm

Experimental Setup

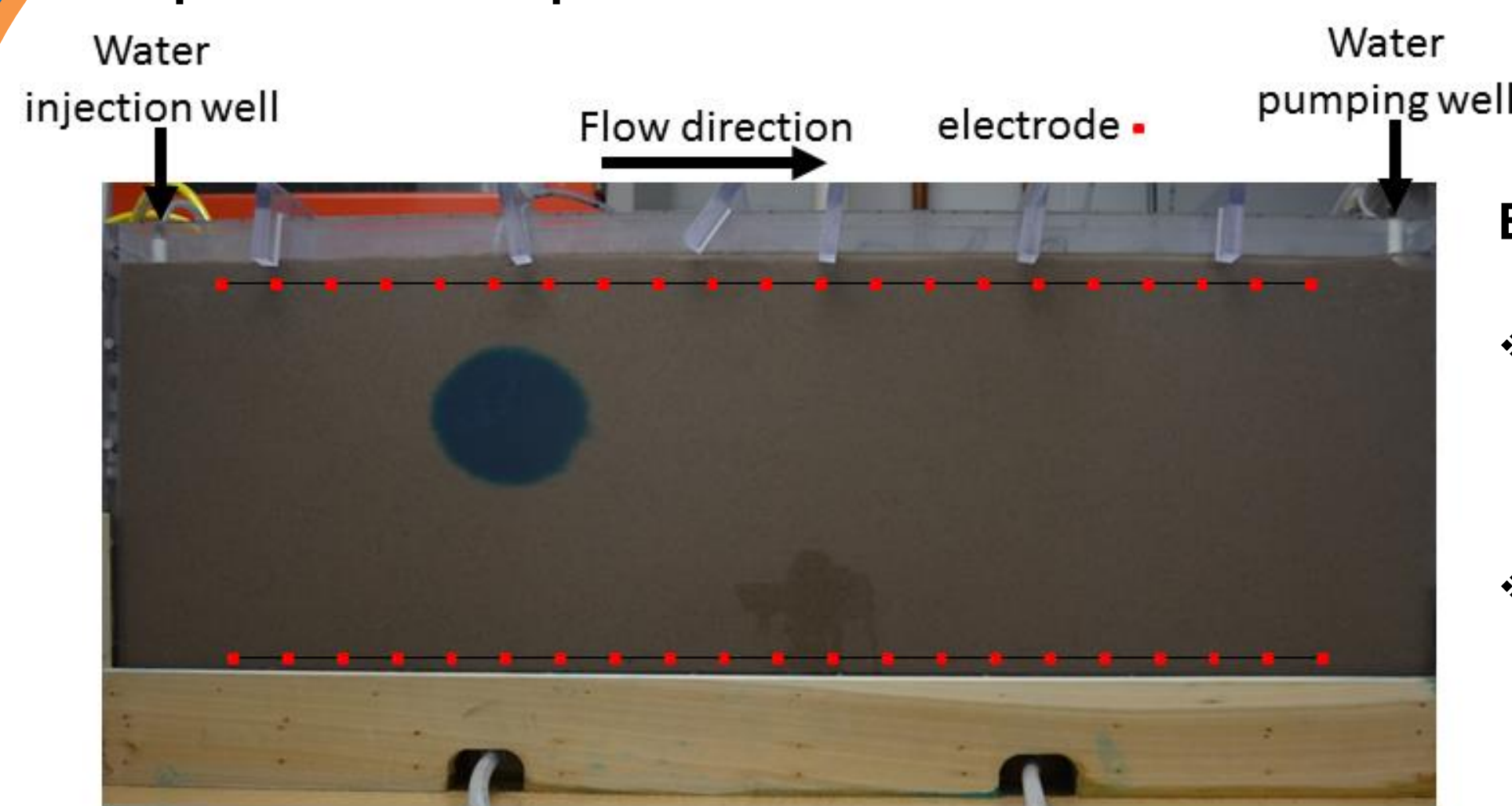


Figure 2: An image of the lab-scale sandtank filled with homogeneous fine sand.

METHODS

Experimental Procedure

- ❖ Injection tracer dyed with brilliant blue to enable video monitoring of the experiment.
- ❖ Single and double sources pulse injections to generate unimodal and bimodal target plume morphologies, respectively

Resistivity Survey

- ❖ The horizontal borehole orientation (Fig. 2) was used to provide good aspect ratio for the resistivity survey while enabling a long horizontal tracer migration field.
- ❖ Circulating dipole-dipole with reciprocal measurements to acquire 3576 quadruples for each survey.
- ❖ FW2_5D [*Pidlisecky and Knight, 2008*] was used for the resistivity forward simulations.

- ❖ The same set of 300 optimal basis vectors (Fig. 3) were employed for the reconstruction of both the unimodal and bimodal target plumes.
- ❖ The locations of the basis patterns were fixed at the center of the domain for all reconstructions.

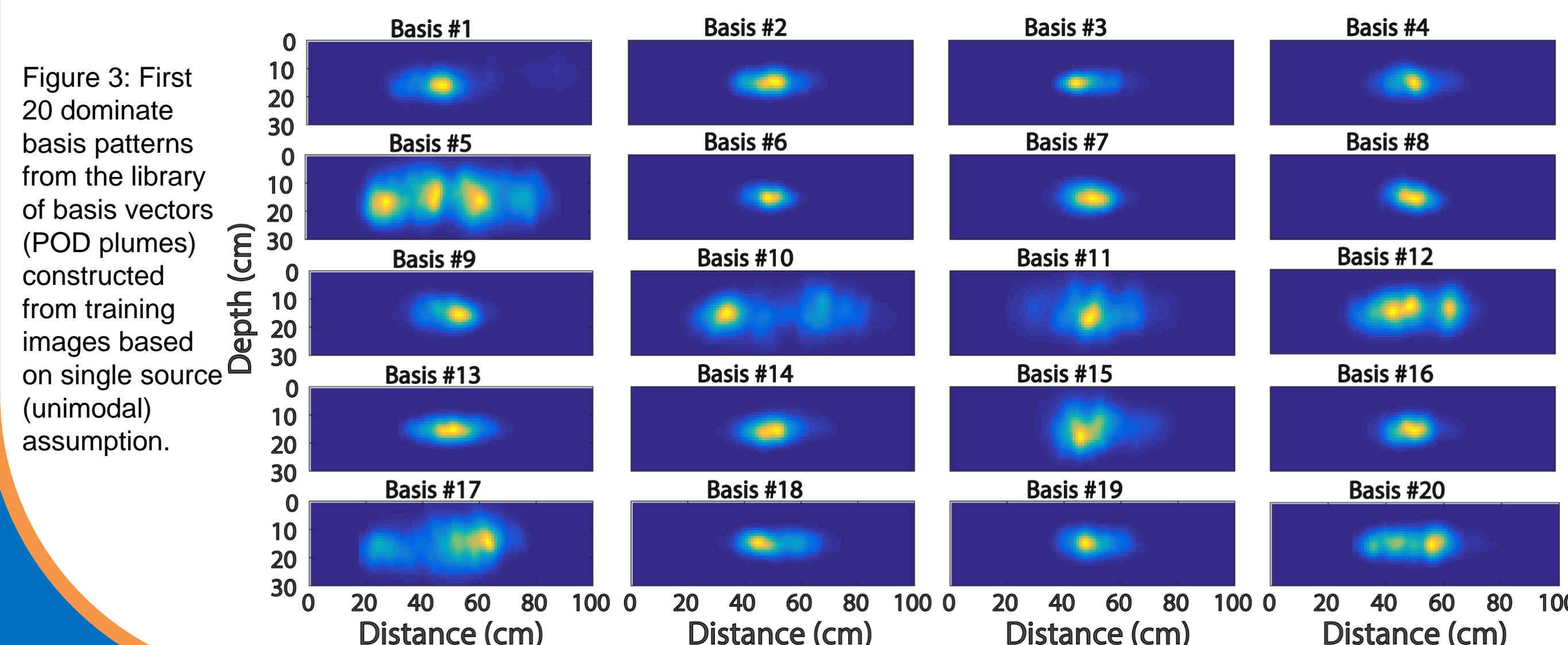


Figure 3: First 20 dominate basis patterns from the library of basis vectors (POD plumes) constructed from training images based on single source (unimodal) assumption.

INTRODUCTION

❖ Geophysical monitoring provides spatiotemporal insights into subsurface processes in a rapid and non-invasive manner.

❖ ER imaging requires regularization for tractability due to the inherent limited noisy measurements.

THE PROBLEM STATEMENT

Traditional geophysical regularization constraints are independent of the physics of the underlying process and often produces dispersed solute plumes with mass underestimation.

❖ We present a lab-scale time-lapse demonstration of the Proper Orthogonal Decomposition (POD)-based inversion algorithm (*Oware et al., 2013; Oware and Moysey, 2014*).

❖ The algorithm performs physics-based regularization by constraining the inversion with POD basis tuned to the physics of the target hydrologic process.

RESULTS

❖ Estimated PODTL solute plumes seem more compact with fewer artifacts in contrast to those obtained from CTL (Fig. 4).

❖ While POD under-estimated mass between 8-24%, CTL under- or over-estimated mass between 8-19% (Tab. 1).

❖ Center of mass (μ) estimation appears less sensitive to artifacts (Tab. 1) compared to that of plume size (σ^2) estimation, probably due to the squaring of the effects of artefacts in second moment estimation.

❖ Both PODTL and CTL detected the bimodality in the target but they seem to underestimate one of the plumes at each time-step (Fig. 5).

❖ There is severe mass under-estimation for both methods, with PODTL under-estimating mass between 19-42% and CTL doing same between 46-60% (Tab. 2).

❖ While center of mass seems fairly resolved, there is severe overestimation in the lateral plume size (σ_x^2) for both methods (Tab. 2).

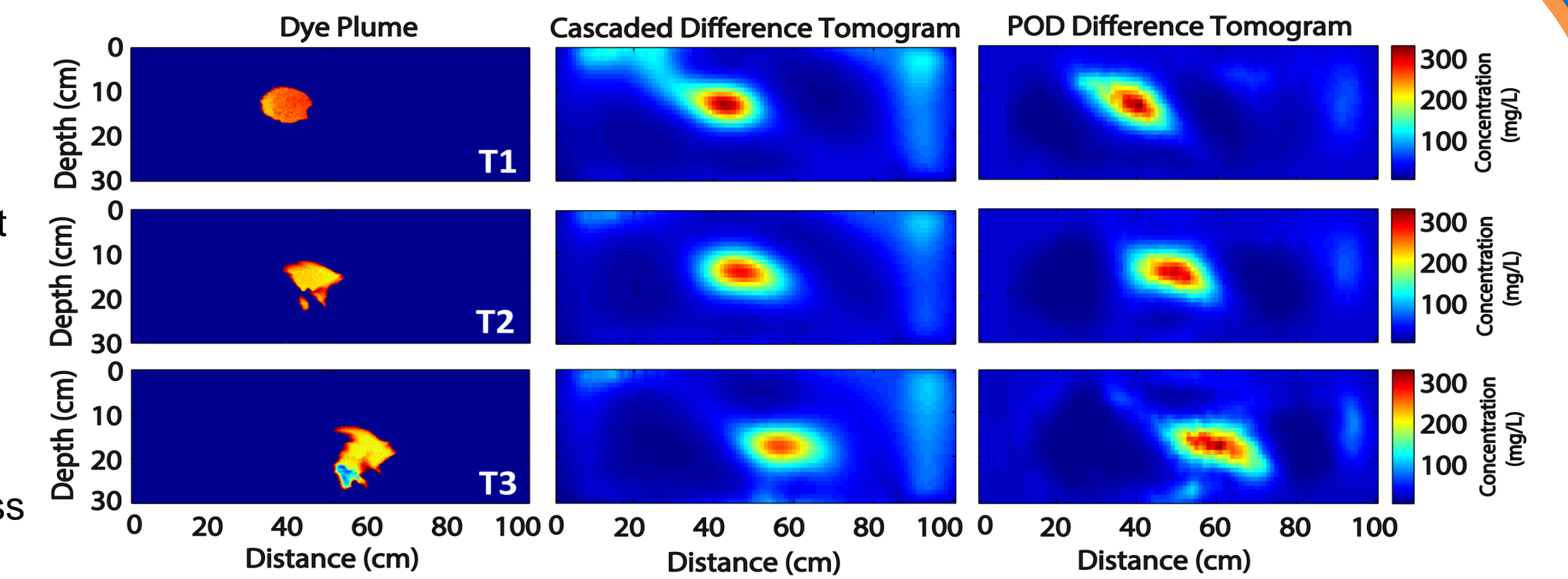


Figure 4: Images of the dye plumes and CTL and PODTL difference tomograms for the unimodal scenario. The dye difference plumes where threshold based on color scale.

Table 1: Results of unimodal plume spatial moments analyses

	Total Mass (mg)	Center of Mass (cm)				Total Mass (mg)	Center of Mass (cm)								
		μ_x	μ_z	σ_x^2	σ_z^2		μ_x	μ_z	σ_x^2	σ_z^2					
		Time-step 1					Time-step 2					Time-step 3			
True Values	155	38.8	12.9	13.8	5.4	155	45.3	16.0	15.6	7.8	155	57.5	19.1	18.7	12.7
Cascaded	168	39.5	11.1	287.2	26.1	127	47.0	14.4	93.7	14.0	142	58.1	17.8	196.6	24.4
POD	118	40.3	13.6	165.6	20.2	112	48.7	15.7	59.1	17.4	143	58.4	18.4	118.5	27.2

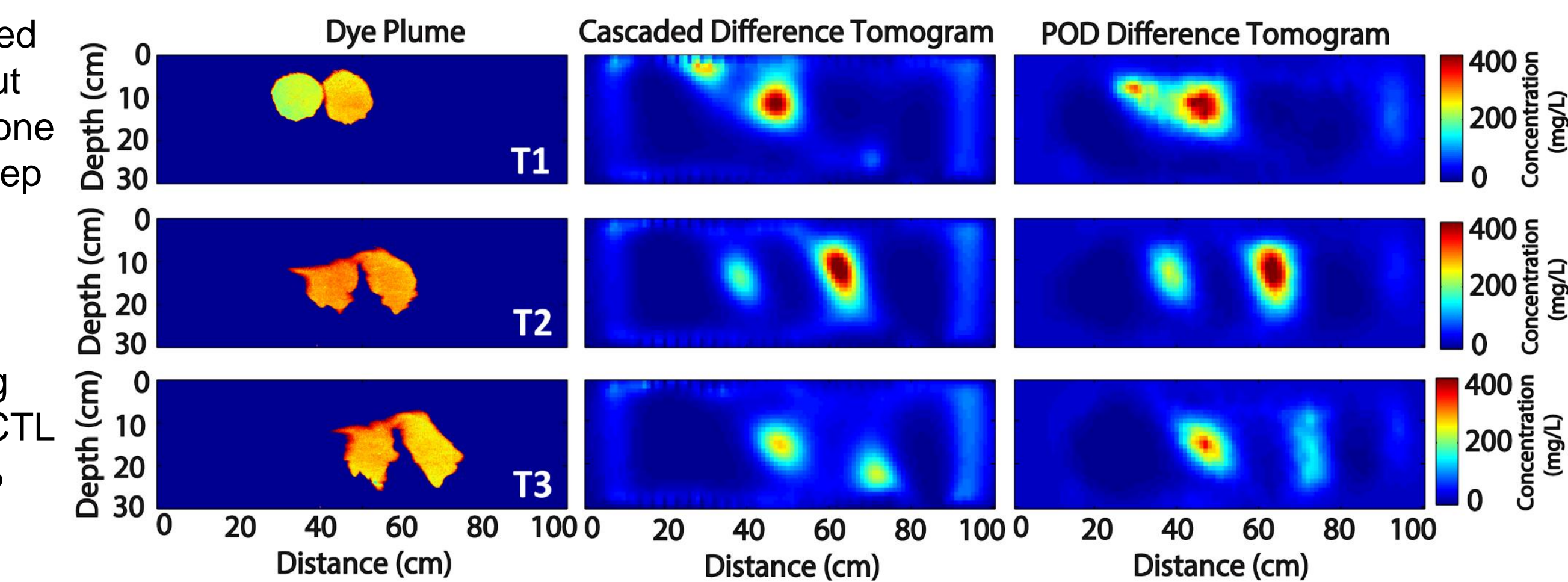


Figure 5: Images of the dye plumes and CTL and PODTL difference tomograms for the bimodal scenario. The dye difference plumes where threshold based on color scale.

Table 2: Results of bimodal plume spatial moments analyses

	Total Mass (mg)	Center of Mass (cm)				Total Mass (mg)	Center of Mass (cm)								
		μ_x	μ_z	σ_x^2	σ_z^2		μ_x	μ_z	σ_x^2	σ_z^2					
		Time-step 1					Time-step 2					Time-step 3			
True Values	254	41.0	9.7	45.4	9.4	254	49.6	14.3	62.7	12.3	254	58.9	15.7	62.8	18.0
Cascaded	138	42.4	9.6	121.5	24.4	129	57.5	13.6	145.5	19.7	101	59.1	17.8	230.6	25.8
POD	207	43.2	12.6	246.2	27.1	170	55.7	14.5	157.6	26.9	145	55.6	17.0	227.1	31.9

CONCLUSIONS

- ❖ PODTL tomograms are more compact with seemingly fewer artefacts compared to those of CTL.
- ❖ PODTL mostly outperformed CTL in terms of mass and center of mass estimation with CTL performing slightly better in plume size estimation in the bimodal (inaccurate prior assumption) test case.
- ❖ Plume size estimation is more sensitive to inversion artefacts compared to the influence of artefacts on center of mass estimation.
- ❖ PODTL achieved 90% truncation in the dimensionality of the problem, i.e., estimated 300 coefficients to reconstruct 3000 model parameters.
- ❖ **PODTL is computationally superior requiring less than 5 mins to complete each inversion compared to about 3 hours for CTL to do same.**

REFERENCES

- ❖ Oware, E. K., Moysey, S. M. J., & Khan, T. (2013). Physically based regularization of hydrogeophysical inverse problems for improved imaging of process-driven systems. *Water Resources Research*, 49(10), 6238-6247.
- ❖ Oware, E. K., & Moysey, S. M. J. (2014). Geophysical evaluation of solute plume spatial moments using an adaptive POD algorithm for electrical resistivity imaging. *Journal of Hydrology*, 517, 471-480.
- ❖ Pidlisecky, A., and R.J. Knight (2008), FW2_5D: A MATLAB 2.5-D electrical resistivity modeling code. *Computers & Geosciences*, 34(12), 1645-1654.